3D SEGMENTATION OF FULL WAVEFORM LIDAR DATA FOR SINGLE TREE DETECTION USING NORMALIZED CUT

J. Reitberger [a, *], Cl. Schnörr [b], P. Krzystek [a], U. Stilla [c]

[a] Dept. of Geoinformatics, University of Applied Sciences Muenchen, 80333 Munich, Germany- (josef.reitberger, krzystek)@hm.edu
[b] Dept. of Computer Science and Mathematics, University of Applied Sciences Muenchen, 80335 Munich, Germany- schnoerr@cs.hm.edu
[c] Photogrammetry and Remote Sensing, Technische Universitaet Muenchen, 80290 Munich, Germany- stilla@tum.de

Commission III, WG III/3

KEY WORDS: LIDAR, Segmentation, Aerial Survey, Clustering, Forestry

ABSTRACT:

The study highlights a novel method to segment single trees in 3D from dense airborne full waveform LIDAR data using the normalized cut segmentation. The key idea is to subdivide the tree area in a voxel space and to setup a bipartite graph which is formed by the voxels and similarity measures between the voxels. The normalized cut segmentation divides the graph hierarchically into segments which have a minimum similarity among each other and whose members (=voxels) have a maximum similarity. The solution is found by solving a corresponding generalized eigenvalue problem and an appropriate binarization of the solution vector. We applied the method to small-footprint full waveform data that have been acquired in the Bavarian Forest National Park with a mean point density of 25 points per m^2 in leaf-off situation. The segmentation procedure is evaluated in different steps. First, a linear discriminant analysis shows that the mean intensity of the voxels derived from the full waveform data contributes significantly to the segmentation of deciduous and coniferous tree segments. Second, a sample-based sensitivity analysis examines the best value of the most important control parameter that stops the division process of the graph. Third, we show examples how the segmentation can cope with even difficult situations. We also discuss examples showing the limits of the current implementation. Finally, we present the detection rate of the new method in controlled tests using reference data. If we compare the new method to a standard watershed-based segmentation approach the overall improvement for all tree layers is 9%. However, the biggest improvement can be achieved in the intermediate layer with 14% and in the lower layer with 16% showing clearly the advantage of the new approach to a 3D segmentation of single trees.

1. INTRODUCTION

Laser scanning has been applied for forest inventory in area based methods (e.g. Naesset et al. 2004) and in single tree detection methods to estimate forest parameters like stem volume and tree species distribution. For instance, the study of Persson et al. (2002) reports on a detection rate of 71% for a typical Scandinavian forest type. Heurich (2006) demonstrates that the segmentation method of Persson et al. (2002) leads to a detection rate of 45% in the Bavarian Forest National Park. Timber volume is usually estimated from the tree height and crown diameter. The afore mentioned study of Persson et al. (2002) reports that 91% of the timber volume could be determined with 22% RMSE. Heurich (2006) estimates 85% of the timber volume with 31% RMSE.

Most of the methods for single tree detection have in common to find the trees from local maxima in the canopy height model (CHM). The stem position usually corresponds with a peak in the CHM, and the crown diameter is basically found from the segment polygon which is delineated from the CHM surface. The methods from Hyyppä et al. (2001), Solberg et al. (2006) and Brandtberg (2007) stand for this fundamental approach that has the drawback to solely use the CHM. Furthermore, the mandatory smoothing of the CHM smears out local maxima of neighbouring trees. Since smaller trees below the canopy do not appear in the CHM the detection rate of trees with small diameter at breast height (DBH) is considerably low. Maltamo et al. (2004) developed a procedure to predict small occluded trees in lower forest levels by theoretical distribution functions. Timber volume and stem density can be estimated with 16% RMSE and 49% RMSE, respectively. The distribution functions must be calibrated with field data. Recently, Wang et al. (2007) presented a new method for 3D reconstruction of trees and tackled the problem with a hierarchical morphological approach. The 3D segments of trees are found by combining hierarchically the individual 2D tree crown regions detected in each layer of a voxel space.

In general, the single tree approach has some clear advantages. If successfully applied, it provides not only tree species information and estimates timber volume but also allows the evaluation of the habitat and the biodiversity of forests. However, Maltamo et al. (2007) point out that single tree detection methods need to be more accurate than standard forest inventory methods assuming that reduced cost must not be the only driving force to replace standard methods. The study shows that timber volume can only be estimated with about

* Corresponding author.

30% RMSE accuracy if derived as a function of the tree height and the crown diameter. Clearly, the parameter DBH is not a deterministic parameter but also dependent from many other parameters which are not of allometric nature. Thus, in view of the apparent advantages of single tree methods the detection rate of single trees and the accuracy of tree species classification must be improved. New technologies like small footprint full waveform systems will be one new driving force to push the methods to a new level since they detect significantly more reflections in the tree crown and provide the intensity and the pulse width as reflecting parameters. Moreover, new reconstruction methods for single trees must truly work in 3D and must be flexible to use various types of information modern LIDAR technologies provide.

The objective of this paper is (i) to present a new method that segments single trees in 3D with the normalized cut segmentation and adaptively incorporates reflecting parameters of trees, (ii) to demonstrate with a discriminant analysis how the mean intensity and mean pulse width derived from the full waveform data contribute to the segmentation result, (iii) to show in various examples how the segmentation works, and (iv) to explain experimental results about the improved detection rate of small trees in the lower layer.

The paper is divided into five sections. Section 2 highlights the normalized cut segmentation of the single trees. Section 3 shows the results which have been obtained from full waveform data acquired in May 2006 by the Riegl LMS-Q560 scanner in the Bavarian Forest National Park. Finally, the results are discussed with conclusions in section 4 and 5.

2. METHODOLOGY

2.1 Preprocessing of LIDAR data

Let us assume that full waveform LIDAR data have been captured in a region of interest (ROI). A single waveform is decomposed by fitting a series of Gaussian pulses to the waveform which contains N_R reflections (Figure 1a).

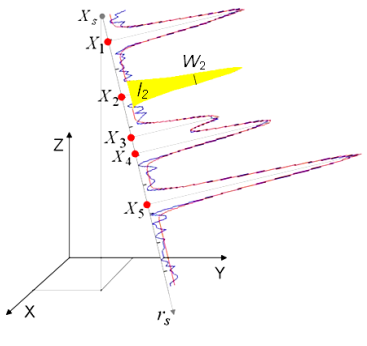

Figure 1a. 3D points, intensity and pulse width derived from a waveform

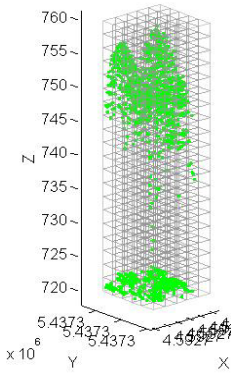

Figure 1b. Subdivision of ROI into a voxel structure

The vector $\boldsymbol{X}_i^T = (x_i, y_i, z_i, W_i, I_i)(i = 1,..., N_R)$ is provided for each reflection i with the coordinates (x_i, y_i, z_i) as the 3D position of the reflection. Additionally, the points $\boldsymbol{X}_i$ are given the pulse width W_i and the intensity parameter I_i of the return pulse. These parameters are calibrated with respect to the pulse width and intensity of the emitted signal and the travelling distance (Jutzi and Stilla 2005, Reitberger et al. 2006). Note that I_i is the integral of the Gaussian function which corresponds to the pulse energy of the reflection.

The ROI is subdivided into a voxel structure with a voxel spacing of vp and $N_V = N_v^x \, x \, N_v^y \, x \, N_v^z$ voxels (Figure 1b). Within each voxel (l,m,n) $(l = 1,.., N_v^x;\ m = 1,.., N_v^y;\ n = 1,.., N_v^z)$ of size vp^3 we collect N_{lmn} reflections $\boldsymbol{X}_i^T = (x_i, y_i, z_i, W_i, I_i)(i = 1,..., N_{lmn})$. Furthermore, we apply a watershed-based segmentation (Reitberger et al. 2007) in the ROI to the CHM and assign the local maxima of the segments to possible stem positions $\boldsymbol{X}_{stem_i}^T = (x_{stem\,i}, y_{stem\,i})$ $(i = 1,..., N_{stem})$.

2.2 Segmentation

The 3D segmentation of trees is based on the normalized cut segmentation which has been introduced by Shi and Malik (2000) in image analysis. The voxel space is represented as a graph $G = \{V,E\}$ with V as the voxels representing the nodes and E as the edges formed between every pair of nodes. The similarity between two nodes $\{i,j\} \in V$ is described by the weights w_{ij} which are computed from features associated with the voxels. Basically, the similarity between voxels decreases with increasing distance between two voxels and drops down to zero beyond a certain threshold in order to keep the graph G at a reasonable size for computational reasons. The goal of the normalized cut segmentation is to divide the graph G into disjoint voxel segments A and B by maximizing the similarity of the segment members and minimizing the similarity between the segments A and B.

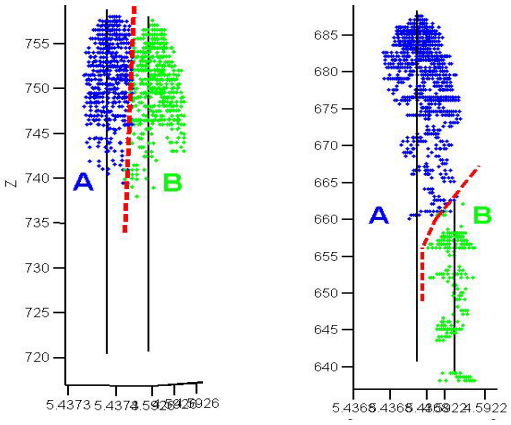

Figure 2. Voxels containing tree reflections and the division into two tree segments A and B.

The corresponding cost function is

$$NCut(A,B) = \frac{Cut(A,B)}{Assoc(A,V)} + \frac{Cut(A,B)}{Assoc(B,V)} \qquad (1)$$

with $Cut(A,B) = \sum_{i \in A, j \in B} w_{ij}$ as the total sum of weights between the segments A and B and $Assoc(A,V) = \sum_{i \in A, j \in V} w_{ij}$ representing the sum of the weights of all edges ending in the segment A. The minimization of *NCut(A,B)* is solved by the corresponding generalized eigenvalue problem

$$(D - W)y = \lambda Dy \quad (2)$$

The $n \times n$ weighting matrix W is representing the weights w_{ij} between all nodes n of the graph G and is usually positive definite. The $n \times n$ degree matrix D is directly derived from W and holds the degree of a node i at the diagonal element $D(i,i) = \sum_j w_{ij}$. The minimum solution y_1 for (2) corresponds to the second smallest eigenvalue λ_1. Since y_1 may only have two distinct indicator values (+1,-1) we need to discretize it by introducing a threshold $thres_{Ncut}$ into the histogram of the real-valued vector y_1 (Messner, 2007). This essentially subdivides the graph G into two disjoint segments A and B. Finally, the subdivision of the graph G into several segments is found in the following hierarchical procedure.

Step 1: Create the graph G by computing W and D for all nodes.
Step 2: Find the solution of the eigenvalue problem (2).
Step 3: Binarize the solution vector y_1 with $thres_{Ncut} = 0$ and cut the graph G into two new graphs G_1 and G_2 if the number of voxels for each graph is larger than a certain number of voxels.
Step 4: Apply steps 1 to 3 to the graphs G_1 and G_2. Stop if the value for *Ncut* reaches or exceeds the threshold $Ncut_{thres}$.

2.3 Setup of similarity function

In order to set up the weighting matrix W we introduce the function

$$w(i,j) = e^{-F(i,j)} \times e^{-X(i,j)} \times e^{-Z(i,j)} \times e^{-G(i,j)} \quad (3)$$

with

$$F(i,j) = \left(\frac{|f_i - f_j|}{\sigma_f} \right)^2 \quad X(i,j) = \left(\frac{D_{ij}^{XY}}{\sigma_{xy}} \right)^2$$

$$Z(i,j) = \left(\frac{D_{ij}^{Z}}{\sigma_z} \right)^2 \quad G(i,j) = \left(\frac{G_{ij}^{\max}}{\sigma_G} \right)^2 \quad (4)$$

that computes the similarities w_{ij} between two voxels i and j. The key idea of function (3) is to multiplicatively combine several impact factors on the similarity in dependence on the distance between the voxels. The component *F(i,j)* describes the quadratic Euclidian distance between two feature vectors f_i and f_j derived from the data points (=reflections) in the voxels. The components *X(i,j)* and *Z(i,j)* weight the quadratic Euclidian distances between the voxels, where D_{ij}^{XY} is the horizontal and D_{ij}^{Z} the vertical distance. The horizontal and vertical distances are weighted separately to take into consideration the prior knowledge of a typical 3D tree shape. Finally, the fraction *G(i,j)* uses the stem positions $\boldsymbol{X}_{stem}^{T}$, if available, and weights voxels in dependence on their maximum distances $G_{ij}^{\max}$ to $\boldsymbol{X}_{stem}^{T}$. This renders possible to introduce tree locations derived from other methods, e.g. a 2D watershed-based segmentation or a 3D stem detection procedure. The parameters σ_f, σ_{xy}, σ_z and σ_G control the sensitivity of the impact factors *F(i,j)*, *X(i,j)*, *Z(i,j)* and *G(i,j)* (4) in the numerator.

Finally, we introduce the features $f_i = \{I_{mean}, W_{mean}\}$ for each voxel i which are calculated from the N reflections in a given space segment S of size 2m x 2m x 6m as

$$I_{mean} = \frac{1}{N} \sum_{j \in S} I_j \qquad W_{mean} = \frac{1}{N} \sum_{j \in S} W_j \quad (5)$$

The features in (5) are representing the mean intensity and the mean pulse width for each voxel. The computation in (5) is equivalent to a low pass filtering of the raw reflections with a box filter.

2.4 Postprocessing of segments

The result of the normalized cut segmentation is cleaned in the following steps. Firstly, each segment whose number of voxels goes below the value of 30 is cancelled. Secondly, we subdivide each segment into layers of height 2.0 m and search for layers containing only empty voxels (=no reflections!) at an absolute segment height of more then 10 m. All the voxels above the empty layer are ignored.

2.5 Control parameters

The normalized cut segmentation is controlled by several control parameters whose values have been optimized in experiments. Firstly, the size of the voxels *vp* was set equal to 0.5 m. The most important parameter $Ncut_{thres}$, which controls the subdivision (=cut) of a graph G, was set equal to 0.16. Moreover, a graph G in step 3 is not subdivided anymore if the number of voxels of the graph undershoots the limit of 40 voxels. Finally, we used the empirical values $\sigma_f = 0.5$, $\sigma_{xy} = 1.35$ m, $\sigma_z = 11.0$ m and $\sigma_G = 3.5$ m to control the influence of the impact factors *F(i,j)*, *X(i,j)*, *Z(i,j)* and *G(i,j)*. The value for σ_z is larger than σ_{xy} assuming that the tree height is larger than the tree crown diameter.

3. EXPERIMENTS

3.1 Material

Experiments were conducted in the Bavarian Forest National Park (49° 3' 19" N, 13° 12' 9" E). 18 sample plots with an area size between 1000 m^2 and 3600 m^2 were selected in the mixed mountain forests. Reference data for all trees with DBH larger than 10 cm have been collected in May 2006 for 688 Norway spruces (*Picea abies*), 812 European beeches (*Fagus sylvatica*), 70 fir trees (*Abies alba*), 71 Sycamore maples (*Acer pseudoplatanus*), 21 Norway maples (*Acer platanoides*) and 2 lime trees (*Tilia europaea*). Tree parameters like the DBH, total tree height, stem position and tree species were measured and determined by GPS, tacheometry and the 'Vertex III' system. Full waveform data have been collected by Milan Flug GmbH with the Riegl LMS-Q560 scanner in May 2006 after snowmelt but prior to foliation with an average point density of 25 points/m^2 at a flying height of 400 m. The procedures for the normalized cut segmentation were applied to all the plots in a batch procedure without any manual interaction. Note also that

reference trees are plotted in the figures 2, 4, 5, 7, 8 and 9 as black vertical lines.

3.2 Linear discriminant analysis

In order to test the statistical contribution of the features I_{mean} and W_{mean} to the segmentation process a linear discriminant analysis was applied in advance to voxels in selected segments for which the tree species were exactly known. The segments were subdivided into pairs of segments representing the possible combinations of tree species. In total, the test data set comprised 372 pair combinations with 39% deciduous-deciduous pairs, 21% deciduous-coniferous pairs and 40% coniferous-coniferous pairs. Thereafter, we calculated the features I_{mean} and W_{mean} in the known segments for all voxels forming a characteristic group of features for each tree species. Finally, a multivariate normal density function was fitted to all the groups with a pooled estimate of the covariance yielding finally an average classification error for each tree species combination. The results depicted in figure 3 show that the mean pulse width W_{mean} classifies each tree species combination with an overall accuracy of 67%. The mean intensity I_{mean} works in general better than the pulse width and reaches – as expected - the best result for the combination deciduous-coniferous. Thus, the mean intensity collected in a tree segment contributes significantly to the segmentation process.

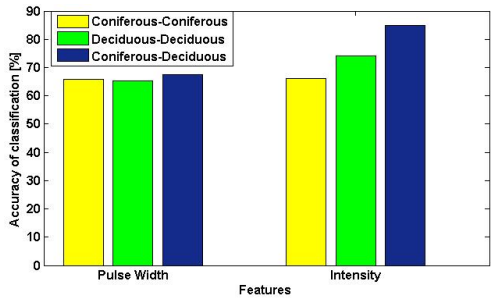

Figure 3. Result of discriminant analysis for voxels of correctly segmented trees

3.3 Sensitivity analysis of control parameters

The important $Ncut_{thres}$ value controls the subdivision of the segments in step 4 of the segmentation procedure. The larger the value is set the higher is the similarity between the resulting segments. The figures 4 and 5 show in an example how the value 0.16 splits the upper right (yellow) segment into two correct tree segments.

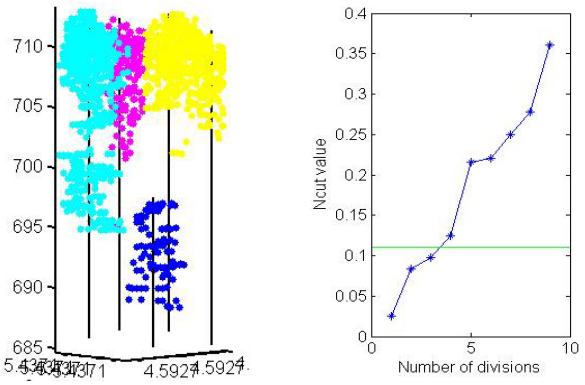

Figure 4. Tree segments resulting from an *NCut* value of 0.11

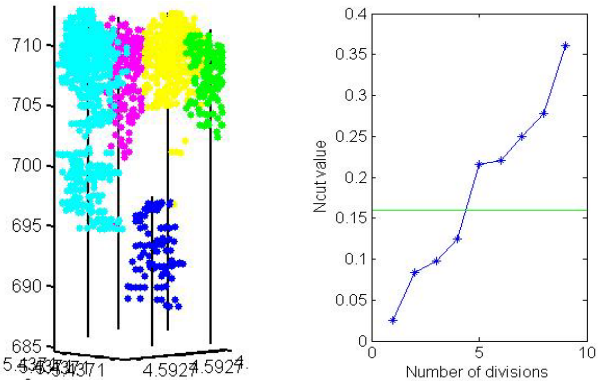

Figure 5. Tree segments resulting from an *NCut* value of 0.16

Note that the higher the value of $Ncut_{thres}$ is set the better is the detection rate of single trees. However, this leads normally also to a larger number of false positives. This is nicely depicted in figure 6 where the sensitivity of the segmentation process in terms of correctly found trees and false positives is shown. The value of 0.16 was found as the best compromise and – more important – was robust for all the reference areas. Tests with data sets from other ALS campaigns (different sensors and point densities) showed also that a value around 0.16 is optimal. The other control parameters of section 2.5 proved to be robust, too. However, slight modifications are worthwhile to get optimal results for the different data sets. An automatic estimation of the control parameters e.g. in dependence on the point density appears complex and was postponed for the time being.

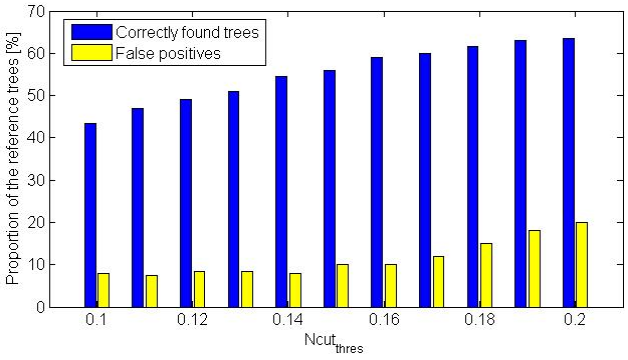

Figure 6. Influence of control parameter $Ncut_{thres}$ on detection rate and false positives

3.4 Normalized cut segmentation

In general, the normalized cut segmentation was able to cope with even complex situations as shown for instance in figure 7. Small trees below the crown of a tall tree or even tree groups in close neighbourhood could be clearly separated.

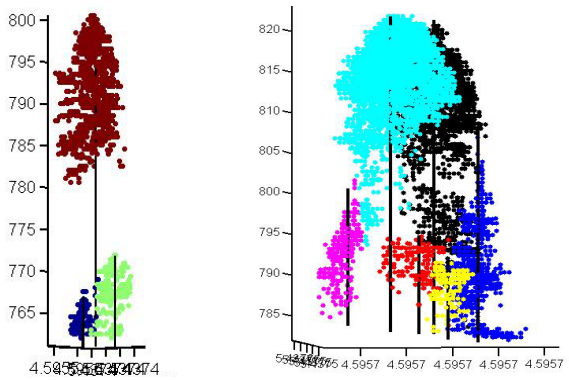

Figure 7. Examples for excellent segmentation results

Of course, there are still critical situations the segmentation procedure could not sufficiently solve – for instance – if trees grow in fairly close neighbourhood like in figure 8. In the left plot the normalized cut segmentation could only segment two trees instead of seven trees. The right plot shows a group of five trees which are merged to one segment. The trees are standing close together and are forming a homogeneous indivisible point cloud. But remarkably, at least the small groups of trees in the left plot of figure 8 could be detected. This seemed to be impossible so far in segmentation methods that are solely using the CHM. The reasons for false tree segments are manifold. The left plot in figure 9 shows that the segmentation wrongly assigns branches of the tall tree to the smaller tree beneath this tree. Thus, the smaller segment is completely inaccurate and the segment of the tall tree is falsified. The right plot shows two broad trees whose crowns are partly merged to a third segment for which a reference tree does not exist. An increase of the control parameter σ_{xy} might solve this problem. However, the drawback of this parameter change would be that smaller trees are merged to one tree, hence increasing the number of non detected trees.

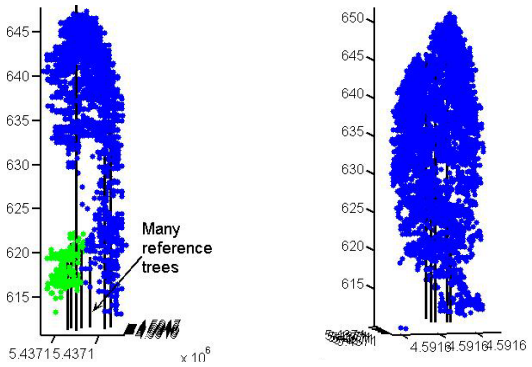

Figure 8. Examples for non detected reference trees

3.5 Results

The accuracy and reliability of the presented single tree segmentation is evaluated in the following. Table 1 contains the percentage of "detected" trees for all reference areas. The trees are subdivided into 3 layers with respect to the mean height h_{mean} of the highest hundred trees per ha. The lower layer contains all trees below 50% of h_{mean}, the intermediate layer refers to all trees between 50% of h_{mean} and 80% of h_{mean}, and, finally, the upper layer contains the rest of the trees.

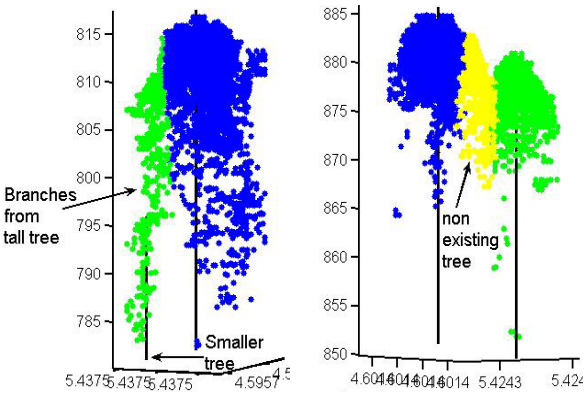

Figure 9. Examples for false segments

Number of reference trees in lower layer		417
Number of reference trees in intermediate layer		356
Number of reference trees in upper layer		891
Percentage of deciduous [%]		54
2D Watershed segmentation	Detected trees lower layer [%]	4
	Detected trees intermediate layer [%]	22
	Detected trees upper layer [%]	78
	Total number of detected trees [%]	47
	False detected trees [%]	5
3D Normalized cut segmentation	Detected trees lower layer [%]	20
	Detected trees intermediate layer [%]	36
	Detected trees upper layer [%]	81
	Total number of detected trees [%]	56
	False detected trees [%]	8

Table 1: Detection of single trees in the reference plots

First, we compare in table 1 the detection rate of single trees that are only derived from a CHM using a watershed-based segmentation approach (Reitberger et al. 2007) with the detection rate of the normalized cut segmentation. As expected, the detection rate is in the order of 80% in the upper layer. In this layer, there is almost no difference between the two approaches. The normalized cut segmentation is slightly better by 3%. However, if we compare the detection rates for the other layers the normalized cut segmentation is significantly superior to the watershed-based approach. In detail, the improvement is 12% for the intermediate layer and 16% for the lower layer. The overall improvement for all layers and all plots is 9%. Finally, the figures 10 and 11 graphically show the detection rates in dependence on the DBH and the tree species.

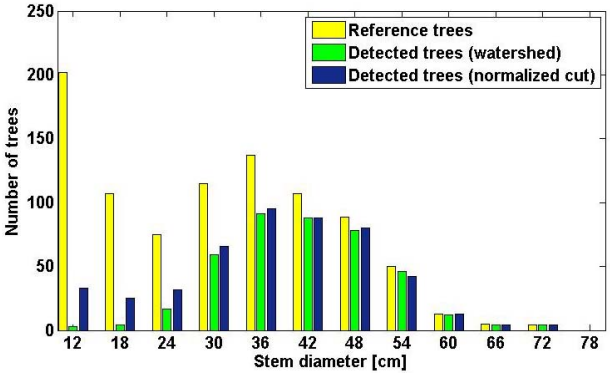

Figure 10. Results of single tree detection for deciduous trees

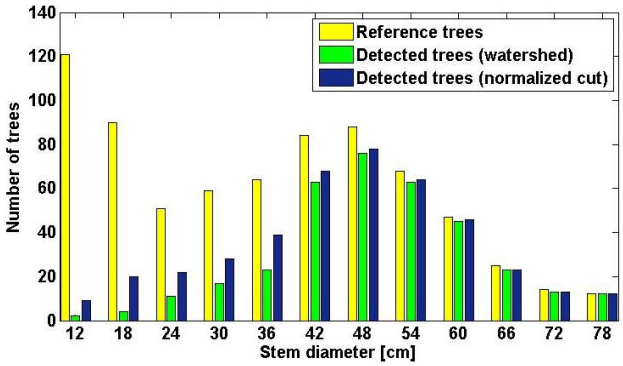

Figure 11. Results of single tree detection for coniferous trees

4. DISCUSSION

The presented approach provides 3D segments of single trees and goes conceptually one step further in comparison to methods which segment tree crowns solely with the CHM. It determines a natural hierarchical segmentation based on an energy minimization and computes thereby approximately a global minimum. Especially, the detection rate for single trees in the intermediate and lower layer is significantly improved. Also, we have demonstrated in controlled tests that the algorithm can even discern trees that either do not appear as isolated maxima in the CHM or are dominated by a large tree. Thus, a direct computation of the crown volume is possible and, hence, timber volume can be estimated more precisely. Moreover, it is to be expected that the accuracy of tree species classification will be improved since single trees are more accurately modelled and, hence, tree species features are more representative. In comparison to other methods that tackle the tree segmentation in 3D it is important to mention that the normalized cut segmentation needs no seed points for the initialization and fully works in 3D. For instance, Morsdorf et al. (2003) use the local maxima of the CHM to initialize a k-means 3D clustering of LIDAR data points. The approach from Wang et al. (2007) firstly splits the tree area in layers and finally connects the 2D tree crowns of each layer to a 3D tree model.

The mathematical formulation makes the approach very flexible to use various information derived from LIDAR data. At the moment, the used information is split up into a geometrical part, a feature-based part and a part which uses prior knowledge about probable stem positions. Note that only the geometrical part is mandatory. Thus, our approach works basically also with conventional first/last pulse data and is not dependent on full waveform data or the stem positions. Also, the list of features can be extended arbitrarily. It is remarkable that stem positions could be directly detected from the 3D point cloud by a special method which works efficiently in the intermediate and upper layer (Reitberger et al. 2007). We expect a slight improvement of the overall detection rate from this extension of the algorithm. Other improvements are possible by a sophisticated post processing of the segmentation result using a priori knowledge about trees. For example, segments could not be accepted if their size exceeds tolerances about the tree shape. Also, segments could be tested with respect to closeness.

5. CONCLUSIONS

The study reports on a novel approach to a 3D segmentation of single trees using the normalized cut segmentation. The results show clearly that small trees in the intermediate and lower layer can be detected more accurately than with conventional segmentation procedures. The method can utilize different types of information derived from LIDAR data. Future research should be focused on an improved estimation of timber volume and tree species classification.

ACKNOWLEDGEMENTS

We thank Dr. Marco Heurich and the Administration of the Bavarian Forest National Park for their productive contributions and for giving us the opportunity to use their remote sensing test sites.

REFERENCES

Brandtberg, T., 2007. Classifying individual tree species under leaf-off and leaf-on conditions using airborne lidar. *ISPRS Journal of Photogrammetry and Remote Sensing*, 61, pp. 325 – 340.

Heurich, M., 2006. Evaluierung und Entwicklung von Methoden zur automatisierten Erfassung von Waldstrukturen aus Daten flugzeuggetragener Fernerkundungssensoren. Forstlicher Forschungsbericht München, Nr. 202, ISBN 3-933506-33-6. http://mediatum2.ub.tum.de/. (Accessed February 18, 2007).

Hyyppä, J., Kelle, O., Lehikoinen, M., Inkinen, M., 2001. A segmentation-based method to retrieve stem volume estimates from 3-D tree height models produced by laser scanners. *IEEE Transactions on Geoscience and remote Sensing,* 39:969-975.

Jutzi B., Stilla U. 2005. Waveform processing of laser pulses for reconstruction of surfaces in urban areas. *In: Moeller M, Wentz E (eds) 3th International Symposium: Remote sensing and data fusion on urban areas, URBAN 2005. International Archives of Photogrammetry and Remote Sensing.* Vol 36, Part 8 W27.

Maltamo, M., Eerikäinen, K., Pitkänen, J., Hyyppä, J., Vehmas, M., 2004. Estimation of timber volume and stem density based on scanning laser altimetry and expected tree size distribution functions. *Remote Sensing of Environment 90 (2004),* pp. 319 - 330.

Maltamo, M., Packalén, P., Peuhkurinen, J., Suvanto, A., Pesonen, A., Hyyppä, J., 2007. Experiences and Possibilities of ALS Based Forest Inventory in Finland. *Proceedings of the ISPRS Workshop Laser Scanning 2007 and SilviLaser 2007,* Volume XXXVI, PART 3/W52, 12 – 14th September 2007, Espoo, pp. 270 – 279.

Messner, M. 2007. Normalized Cut Segmentierung mit Airborne Lidar Daten zur Erkennung von Einzelbäumen im Nationalpark Bayerischer Wald. *Master Thesis at the faculty of Geoinformatics, University of Applied Sciences Muenchen*. Unpublished.

Morsdorf, F., Meier, E., Allgöwer, B., Nuesch, D., 2003. Clustering in airborne laserscanning raw data for segmentation of single trees. *Proceedings of the ISPRS working group III/3 workshop 3-D reconstruction from airborne laserscanner and InSAR data Dresden,* Germany 8-10th October, ISSN 1682-1750 VOLUME XXXIV, PART 3/W13, pp. 27 -33.

Naesset, E., 2004. Practical large-scale forest stand inventory using a small-footprint airborne scanning laser. *Scandinavian Journal of Forest Research,* 19, 164 – 179.

Persson, A., Holmgren, J. and Söderman, U., 2002. Detecting and measuring individual trees using an airborne laserscanner. *Photogrammetric Engineering & Remote Sensing* 68(9), pp. 925–932.

Reitberger, J., Krzystek, P., Stilla, U., 2006. Analysis of Full Waveform Lidar Data for Tree Species Classification. *Symposium ISPRS Commission III "Photogrammetric Computer Vision" PCV06*, 20 – 22th September, Bonn, Germany.

Reitberger, J., Krzystek, P., Stilla, U., 2007. Combined tree segmentation and stem detection using full waveform LIDAR data. *Proceedings of the ISPRS Workshop Laser Scanning 2007 and SilviLaser 2007,*Volume XXXVI, PART 3/W52, 12 – 14th September 2007, Espoo, pp. 332 – 337.

Shi, J., Malik, J., 2000. Normalized cuts and image segmentation. *IEEE Transactions on Pattern Analysis and Machine Intelligence*, 22, pp. 888-905.

Solberg, S., Naesset, E., Bollandsas, O. M., 2006. Single Tree Segmentation Using Airborne Laser Scanner Data in a Structurally Heterogeneous Spruce Forest. *Photogrammetric Engineering & Remote Sensing,* Vol. 72, No. 12, December 2006, pp. 1369-1378.

Wang, Y., Weinacker, H., Koch, B., 2007. Development of a Procedure for Vertical Structure Analysis and 3D-Single Tree Extraction within Forests Based on Lidar Point Cloud. *Proceedings of the ISPRS Workshop Laser Scanning 2007 and SilviLaser 2007,*Volume XXXVI, PART 3/W52, 12 – 14th September 2007, Espoo, pp. 419 – 423.